# The effect of the supramolecular network of (*Z*)-3-(4-(diphenylamino)phenyl)-2-(pyridin-2-yl)-acrylonitrile on the fluorescence behavior of a single crystal: experimental and theoretical studies

M. Judith Percino[1,*], Margarita Cerón[1], Guillermo Soriano-Moro[1], M. Eugenia Castro[1], Víctor M. Chapela[1], José Bonilla[2], Marisol Reyes-Reyes[3] and Román López-Sandoval[4]

[1] Lab. de Polímeros, Centro de Química, Instituto de Ciencias, Universidad Autónoma de Puebla, Complejo de Ciencias, ICUAP, Edif. 103H, 22 Sur y San Claudio, C.P. 72570 Puebla, Puebla, México

[2]Cento de Investigación en Materiales Avanzados S.C.(CIMAV-Unidad Monterrey), Av. Alianza Norte 22, Autopista Monterrey-Aeropuerto Km 10, PIIT, Apodaca-Nuevo León, México, C.P. 666600

[3] Universidad Autónoma de San Luis Potosí, Instituto de Investigación en Comunicación Óptica. Av. Karakorum 1470, C.P. 78210, San Luis Potosí, S.L.P. México

[4] Instituto Potosino de Investigación Científica y Tecnológica, Camino a la Presa de San José N° 2055, C.P. 78216, San Luis Potosí, S.L.P. México.

**Corresponding author:**
M. Judith Percino; judith.percino@correo.buap.mx;
Centro de Química,
Instituto de Ciencias,
Universidad Autónoma de Puebla,
Complejo de Ciencias ICUAP, Edif. 103H,
22 Sur y San Claudio, C.P. 72570
Puebla, Puebla, México

Tel. +52-222-2295500 x 7285,
Fax: +52-222-2295551 in Mexico

## Abstract

The molecular structure and molecular interactions of α,β-unsaturated nitrile, such as the interaction between adjacent molecules of (*Z*)-3-(4-(diphenylamino)phenyl)-2-(pyridin-2-yl)-acrylonitrile (***Z*-DPPyACN**) throughout the 4-diphenylamino moiety with the phenyl and pyridyl rings, play an important role on self-assembly behaviors and optical properties of its powder and single crystal forms. The crystal packing exhibits multiple C−H···π and CH···HC edge-to-face interactions that contribute to the supramolecular network between adjacent molecules. The resulting molecular structure resembles a pinwheel which exhibits a stronger emission intensity at three different wavelengths. The crystal belongs to the monoclinic, space group $P2_1/n$, with dimensions $a$ = 12.955(2), $b$ = 11.2900(15), $c$ = 14.6992(3) Å, $\beta$ = 115.648(2)°, and Z=4. The single crystal compound shows three emission maxima at 533, 569, and 607 nm, whereas the powder and the molecules in the aggregate state show maximum emission intensities that are dependent on the nature of the solvent. The ***Z*-DPPyACN** dye optical properties show a Stokes shift caused by a reorganization of the molecule in the excited state, as affected by the solvent polarity. This indicates a large change in the dipole moment of dye molecules upon excitation due to an intramolecular charge transfer interaction. For a theoretical point of view, the molecular geometry, the electronic structure, and excitation energies are reported using Density

Functional Theory and compared with the experimentally-determined one photon absorption and emission spectra.

**Keywords:** 4-diphenylamino moiety, crystal structure, fluorescent organic compound, DFT calculations, multiple C−H···π interactions, acrylonitrile derivatives.

## Introduction

Aromatic amines are among the most important reagents used as nanodevice materials,[1-20] and they serve to covalently attach various compounds to light emitting layers.[14,21,22] Furthermore, they have been tested as blue emitters in organic LEDs[23] and as components of electroluminescent bipolar devices.[24]

The use of *N*-phenyl substituents on aromatic amines has resulted in superior performance in materials chemistry.[25-33] For example, the introduction of *N*-phenyl substituents into *trans*-aminostilbene carried considerable bathochromic shifts and high fluorescence quantum yields compared with *N*-alkyl substituents, which suggests a substantial interaction of the *N*-phenyl with the aminostilbene groups (conjugated structure).[34] Yang *et al.*[34] reported that the excited-state process of *N*-phenyl substituents in *trans*-aminostilbene is a consequence of the more planar geometry and strong orbital interactions between the *N*-phenyl and the aminostilbene groups. In the particular case of *p*-diphenylaminostilbene, the compound displayed a second absorption band at shorter wavelengths as well as the single intense long wavelength band, and the former was assigned to *trans*-stilbene. This second band near 300 nm was assigned as a consequence of an electronic transition mainly localized in the triphenylamine moiety. Among the aromatic amines, triphenylamine ($NPh_3$) and its derivatives are very important in photoscience.

These compounds have been used at length as the hole transport material in organic electroluminescent devices.[35-51]

Triphenylamines, with their characteristic propeller starburst molecular structure, have been widely used in opto- and electroactive materials due to their favorable electro-donating and transporting capabilities.[52] These interesting properties have made them the subject of extensive experimental and theoretical studies. It has been suggested that in these materials, the π-conjugation is not disturbed by the central nitrogen atom, and the whole molecule can be considered a chromophore with characteristic absorption and emission properties.[53,54] Sasaki *et al.*[55] showed that $NPh_3$ molecules have C3 symmetry in the gas phase with a C–N–C angle of 116 ± 2°. Jaffe[56] reported the ultraviolet absorption spectra of $NPh_3$ and its methyl derivatives $NPh_{3-n}Me_n$ (n = 1, 2), and identified two absorption bands at similar positions ($NPh_3$: 228 and 297 nm; $NPh_2Me$: 245 and 291 nm; $NPhMe_2$: 252 and 298 nm). Furthermore, replacement of the phenyl group with a methyl group decreased the molar absorption coefficient ($\varepsilon$) of the band at 291–298 nm, and simultaneously increased the $\varepsilon$ of the band at 228–252 nm. Some researchers have proposed that the central $NC_3$ skeleton of nitrogen and the three attached carbon atoms in $NPh_3$ is planar.[1,57] Recently, Sumimoto *et al.*[57] reported on the molecular geometry, electronic structures, and excitation energies of $NPh_3$, $NPh_2Me$, etc. These authors used computational methods to observe that the orbitals of the nitrogen atom overlapped with the π-orbital of the phenyl group in an anti-bonding fashion in the HOMO, and that the orbital energy increased as the overlap increased. The unoccupied orbitals were generated from bonding-type and anti-bonding-type interactions between the π-orbitals of the phenyl groups; therefore, the number of phenyl groups strongly affected the energy diagram of the compounds, which was manifested as a spectral change in the ultraviolet region. In contrast, cyano-substituted (R-C≡N) compounds, with high electron affinities, have shown good optical and electrical properties. The cyano group has high electron affinity and therefore can be used as a buffer layer for the introduction and extraction of electrons in organic devices. Molecules with the electron-withdrawing cyano group on the central phenylene ring are strongly fluorescent.[58] In particular, some cyano-substituted compounds have been reported to show a uniquely enhanced emission rather than fluorescence quenching in the solid state.[59-61] Finally, pyridine is considered an electron acceptor due to its high electron affinity, and has been used in novel bipolar materials[62] as well as electron transporting materials in organic devices.[63-65]

In organic nanostructures based in π-conjugated materials, the noncovalent intermolecular face-to-face π–π interactions (or π–π stacking) play an essential role in crystal engineering and the corresponding tuning of their properties.[66] It is also clear that face-to-face π–π interactions result in cofacial configurations, which increase the amount of π–π orbital overlap and thus are detrimental to luminescence in the organic nanostructures.[67,68] Recent work showed that edge-to-face π−π interactions, termed C−H···π interactions, lead to the formation of interesting organic nanostructures.[66] Although a single C−H···π interaction is kinetically labile and the enthalpy is only about 1.6−2.5 kcal/mol,[46-48] multiple C−H···π interactions could be used to engineer nanoscaled molecular assemblies as well as affect their luminescent behavior.

In this study, we investigated the differences in photophysical properties in the powder, solvent, molecular aggregates, and single crystal forms of (*Z*)-3-(4-(diphenylamino)phenyl)-2-(pyridin-2-yl)acrylonitrile (***Z*-DPPyACN**); see Scheme 1. Also, we characterized two A (powder) and B (crystal) forms of ***Z*-DPPyACN** using X-ray diffraction (XRPD) and differential scanning calorimetry (DSC) techniques in order to detect different possible phases on the title compound.

The ***Z*-DPPyACN** crystal packing exhibited multiple C−H···π and CH···HC edge-to-face interactions that contributed to the supramolecular network between adjacent molecules. This resulted in a molecular structure that resembled a pinwheel and could contribute a compound that exhibits strong emission. The crystal structure, packing analysis, and theoretical studies were conducted systematically to determine which substituents carry nonbonding electrons (*n* electrons) that can cause shifts in the primary and secondary absorptions bands.

## Experimental

### *Synthesis and Crystallization*

2-Pyridylacetonitrile and 4-(*N*,*N*-diphenylamino)phenylaldehyde were acquired from Aldrich Chemical Co. We synthesized the compound ***Z*-DPPyACN** (Scheme 1) following a recently reported general procedure.[69] The compound ***Z*-DPPyACN** was obtained in its single crystal form using the following procedure. First, 0.020 g was dissolved in 10 mL of a mixture of ethylacetate:hexane (3:1). This mixture was then set aside at 4 °C, and crystals were obtained after 5 days.

Batches of **A** form were obtained by recrystallization using the following procedure. The sample isolated from the reaction was recrystallized in cyclohexane by preparing a concentrated solution at a boiling temperature. The solution was filtered through precipitation using an ice bath. The powder was washed with more cyclohexane and was then dried to obtain a yellow powder.

The same procedure was repeated using ethanol as a solvent. The only difference was that, after preparation, the saturated solution was kept at room temperature to precipitate the powder. The powder was also washed with 10 mL of ethanol at room temperature, then filtered and dried to the yellow powder.

The batches of **B** form were obtained as follows. The ***Z*-DPPyACN** compound as a powder (0.3426 g) was dissolved in cyclohexane (8 mL) at a boiling temperature, and the vessel with the solution was set aside at 4 °C. After 24 h, tiny crystals formed and these were set aside for an additional 16 h until an adequate amount of crystals formed. These were subsequently filtered and washed with 10 mL of cyclohexane.

In addition, ***Z*-DPPyACN** compound powder (0.805 g) was dissolved in ethanol (10 mL) at room temperature, and the vessel with the solution was set aside at 4 °C. After 8 days, yellow crystals formed, which were then washed with 3 mL of ethanol.

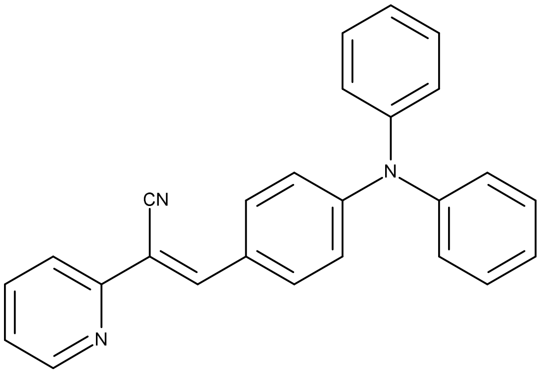

**Scheme 1.** (*Z*)-3-(4-(diphenylamino)phenyl)-2-(pyridin-2-yl)acrylonitrile (***Z*-DPPyACN**).

*Instrumentation*

X-ray crystallography and photolysis properties of ***Z*-DPPyACN**

All reflection intensities of X-ray single crystal diffraction (XRSCD) were measured using a KM4/Xcalibur (detector: Sapphire3) with enhanced graphite monochromated Mo *K*α radiation (λ = 0.71073 Å) using the program CrysAlisPro (Version 1.171.34.44 Oxford Diffraction Ltd., 2010). To refine the cell dimensions, we performed data reduction and analytical numeric absorption corrections based on a multifaceted crystal model using the same program. The structure was solved with the program SHELXS-97 and was refined on $F^2$ (Sheldrick, 2008).[70] The temperature of the collected data was controlled using a Cryojet system (manufactured by Oxford Instruments). The H atoms were placed at calculated positions using the instruction AFIX 43, and the isotropic displacement parameters had values 1.2 times $U$eq of the attached C atoms.

X-ray powder diffraction (XRPD) patterns were recorded with a Bruker AXS D8 advanced diffractometer in the Bragg-Brentano geometry, using graphite monochromated Cu $K\alpha$ radiation ($\lambda$ = 1.5418 Å). The reflection intensities were measured with a NaI scintillator detector.

The absorption and fluorescence spectra were acquired with a Spectrometer SD2000 (Ocean Optics, Dunedin, FL) equipped with a pulse xenon light source PX-2 (Ocean Optics). A laser diode at wavelength of 405 nm was the excitation source for measuring the fluorescence. Spectroscopic grade solvents were used for measurements in solution and they were preliminarily checked for the absence of absorbing or fluorescent impurities within the scanned spectral ranges. The absorption of compounds in powder form was measured with KBr pellets.

Images of the sample at several magnifications were taken under an inverted microscope Olympus GX 51 equipped with a 100 W halogen lamp and polarized slider GX-PO and analyzed GX-AN. Samples were observed at 0° and rotated 90°.

Differential scanning calorimetry (DSC) curves were acquired with a TA Instruments DSC Q200. Typically, 1-2 mg of sample was added to an aluminum pan (Tzero®) and heated at 10 °C/min over the range 25 °C to 195 °C. The sample was cooled at the same rate of 10 °C/min from 195 °C to 25 °C.

Theoretical calculations of the fully optimized geometry and electronic properties of ***Z*-DPPyACN** were performed using Density Functional Theory (DFT) and Time Dependent (TD-DFT) methodology, which was implemented in Gaussian 09 software.[71] We used the hybrid functional B3LYP[72] with 6-31+G(d,p) basis.[73] Some of these results were corroborated with the ORCA program[74] using the hybrid functional PBE0[75,76] and the TZVP basis.[77] The electronic properties of the ***Z*-DPPyACN** crystal were acquired using the VASP package,[78,79] which is an efficient implementation of the DFT on an augmented plane wave basis. The interaction between the valence electrons and ion cores were taken into account using the projector augmented wave method,[80] and we used the hybrid functional PBE0.[75,76] The electronic and structural relaxations of the ***Z*-DPPyACN** crystal were performed using the conjugated gradient algorithm to find the convergence thresholds of $1x10^{-4}$ eV for the energy and $1x10^{-3}$ eV/Å for the forces.

## Results and discussion

### *One photon absorption, emission, and theoretical calculations*

Absorption and fluorescence emission spectra of the title compound were recorded in various non-polar and polar (aprotic and protic) solvents. The electronic absorption spectra acquired for ***Z*-DPPyACN** are shown in Fig. 1(a) and Table 1. An insignificant red shift in the absorption wavelength occurred due to solvent effects. The compound ***Z*-DPPyACN** exhibited two absorption bands. One band, at $\lambda_{max}$ 296-301 nm, corresponded to the $n\rightarrow\pi^*$ transition for the electron transfer from the amine moieties toward the aromatic rings of the 4-diphenylaminophenyl chromophores. This agreed well with *ab initio* calculations using TD-DFT-B3LYP with the 6-31+G(d,p) basis (330.41 nm with f=0.2480) for $S_0\rightarrow S_2$, as implemented in Gaussian 09.[71] The second absorption band, with $\lambda_{max}$ at 417-428 nm, was assigned to the $\pi$-$\pi^*$ transition of the conjugated $RRC{=}CR_2R_2$ segments for the $S_0\rightarrow S_1$ transition (440.30 nm with f=0.9251). The ten lowest excited states were included in the TD-DFT calculations. Moreover, these *ab initio* values were corroborated using TD-DFT ORCA calculations at the PBE0-TZVP theory level, which gave 295 nm with f=0.32 for the $S_0\rightarrow S_2$ transition, and 406 nm with f=1.22 for the $S_0\rightarrow S_1$ transition. The absorption of the powdered form of the compound showed essentially the same behavior, with an absorption band at $\lambda_{max}$ 296-301 nm having a well-defined absorption peak. This was very similar to the absorption band of ***Z*-DPPyACN** in chloroform. A second absorption band had a maximum close to 440 nm; this second band is a broad band shifted toward longer wavelengths. The red shift was related to intermolecular interactions due to the formation of aggregates in the powder.

**Table 1** Photophysical properties of ***Z*-DPPyACN** in different states at room temperature

| ***Z*-DPPyACN** | $\lambda_{abs}$ (nm) | $\lambda_{em}$ (nm) |
|---|---|---|
| Powder | 300, 438 | 534 |
| Powder/KBr | 433 | 525 |
| Single crystal | 296-301, 417-428 | 604, shoulder 567, a little shoulder 659 |
| Gel(THF/water) | - | Broad band 567, |
| Chloroform | 296, 428 | 528, and shoulder 562 |
| Acetone | 296, 416 | - |
| THF | 294, 420 | 569 |
| Methanol | 296, smaller absorption 418.41 | 604, shoulder 567, a little shoulder 659 |

To understand the origin of the differences in the absorption spectra in the molecule—between the solution, powder form, and ***Z*-DPPyACN** crystal—we calculated the absorption bands of both forms using a VASP DFT calculation with PBE0 hybrid functional. Figure 1(b) confirmed that the theoretically-obtained spectra of the molecular forms and the isolated crystal corresponded very well with the experimental absorption spectra.

In the theoretical spectra (Fig. 1b), the band corresponding to the n → π* transition is ~280 nm for both forms, while the band corresponding to the π → π* transitions appeared at 370 nm for the molecular form and at 380 nm for the crystalline form. This shift in the maximum of the absorption band and its broadening in the case of the ***Z*-DPPyACN** crystal are related to the intermolecular interactions between the molecules within the unit cell, as well as the interaction between the molecules of neighboring unit cells. This is reflected in the four first HOMO (HOMO, HOMO-1, HOMO-2, HOMO-3) orbitals (the same for LUMO) corresponding to each of the four molecules of the unit cell. When plotted these are mainly localized in one of the molecules of the unit cell, which can vary up to 0.1 eV at the same **k** point. Furthermore, we calculated the vertical excitations considering only the four molecules in the unit cell of the ***Z*-DPPyACN** crystal, using TD-DFT in the ORCA implementation. This showed the introduction of new absorption states (Table 2) induced by the intermolecular interactions between the molecules forming the crystal.

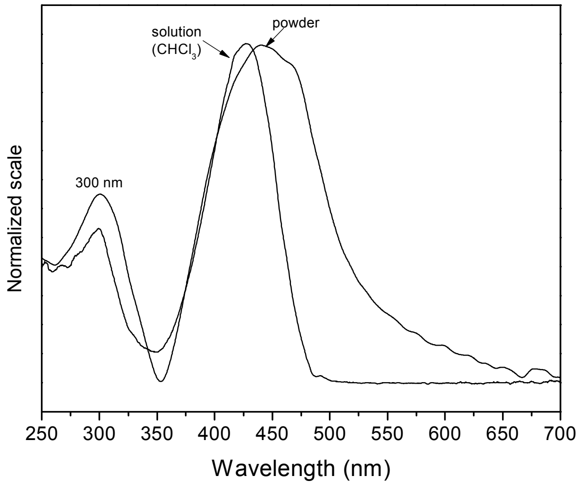

(a)

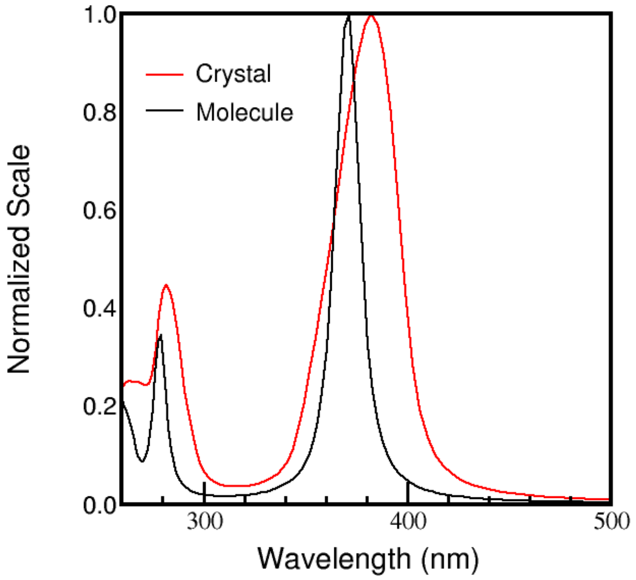

(b)

**Fig. 1** (a) Absorbance spectra of compound ***Z*-DPPyACN** in chloroform and solid state. (b) Theoretically determined absorbance spectra from the ***Z*-DPPyACN** molecule and the single crystal using DFT *ab initio* VASP calculations at the PBE0 theory level.

**Table 2** Absorption spectrum via transition electric dipole moments for ***Z*-DPPyACN**

| State | Energy (cm$^{-1}$) | Wavelength (nm) | $f_{osc}$ | $T^2$ (au$^2$) | $T_X$ (au) | $T_Y$ (au) | $T_Z$ (au) |
|---|---|---|---|---|---|---|---|
| $S_2$ | 21939.9 | 455.8 | 0.009 | 0.134 | -0.094 | -0.257 | -0.244 |
| $S_4$ | 23030.6 | 434.2 | 0.005 | 0.075 | -0.007 | 0.27148 | 0.0336 |
| $S_6$ | 23114.4 | 432.6 | 0.076 | 1.087 | 0.166 | -0.955 | 0.384 |
| $S_8$ | 23268.2 | 429.8 | 0.611 | 8.647 | 0.194 | -2.882 | 0.551 |
| $S_{12}$ | 24260.3 | 412.2 | 3.561 | 48.323 | -1.584 | -0.788 | -6.723 |
| $S_{13}$ | 24350.5 | 410.7 | 0.047 | 0.636 | 0.1886 | -0.066 | 0.772 |
| $S_{18}$ | 31119.2 | 321.3 | 0.0391 | 0.414 | 0.176 | -0.363 | 0.501 |
| $S_{19}$ | 31405.9 | 318.4 | 0.0273 | 0.286 | -0.168 | 0.245 | 0.445 |

$T_X$, $T_Y$, and $T_Z$ are the components of the electric dipole transition moments.

Fluorescence spectra were acquired in the solution, powder, single crystal, and prepared gel nanoparticle forms of the compound using a mixture of THF-$H_2O$ solvent (Fig. 2). The fluorescence spectrum of the compound in chloroform displays a marked red shift due to solvatochromic behavior and a large Stokes shift (Δλst ≈ 110 nm) from strong solvent−solute and dipole−dipole interactions. This was a manifestation of a reorganization of the molecule in the excited state, which led to dissipation of the energy and thus a lowering of the potential energy curve.[2] However, the observed emission spectrum could also be an indication of the formation of a specific solvent-molecule complex, as well as a specific molecule-molecule interaction. The photoluminescence spectra of the molecule in chloroform, as well as in the powder (solid in KBr), showed a strong emission band with maxima at 538 nm. The emission in methanol (a protic and polar solvent) showed a strong emission peak (E3, Fig. 2) at 604 nm, a lower intensity band at 538 nm, and a little shoulder at 659 nm. These are indications of strong solvent-molecule interactions. In addition, a strong Stokes red shift (Δλst ≈180 nm) of the molecule occurred in this solvent due to solvatochromic effects. Solvatochromic shifts reflect extremely complex phenomena involving many different intermolecular forces between the solvent and the molecule.[81] In the TD-DFT calculated emission, we observed a band at 622.48 nm, which is close to one of the experimentally-observed emission bands at 604 nm. From our TD-DFT calculations, we determined that the electric dipole moment of the ***Z*-DPPyACN** molecule in the ground state is **p**=(-0.4902 a.u, 0.911 a.u, 0.936 a.u) with a magnitude of 1.39 a.u. (3.285 Debye); moreover, the electric dipole moment of the excited state after the relaxation process is **p**=(-3.053 a.u., 7.286 a.u, -1.018 a.u.). This large discrepancy in the electrical dipole moment of the ***Z*-DPPyACN** molecule between the ground and excited states is related to the intramolecular charge transfer of the ***Z*-DPPyACN** molecule, which can be observed in the isosurfaces of the frontier molecular orbitals (HOMO and LUMO isosurface models, Fig. 3). Figure 3 shows that the orbital HOMO is localized with the greatest contribution on the amine N atom of the N-diphenyl substitution due to the lone pair electrons. HOMO-1 is localized over the entire molecule, while the LUMO orbital is mainly localized on the pyridine ring and the acrylonitrile group. Intramolecular charge transfer occurs in the molecules during an excitation process, whereby a charge is transferred from a donor part of the molecule to a separate acceptor part of the same molecule. Such molecules are extremely sensitive with respect to the environment and changes in the charge distribution, and they are the origin of large changes in the dipole moments, which in turn alter the interactions with the environment. This process explains the large difference in the emission spectra for the molecule in two different solvents, chloroform and methanol.

The aggregate (gel-nanoparticle) shows a maximum emission (E2, Fig. 2) at 567 nm, and a shoulder at a wavelength similar to the emission maximum for the single crystal at 604 nm. On the other hand, in the solid state (single crystal), the maximum emission (E3) appears at 604 nm in the range of yellow-green light. Small shoulders are also evident at 538 nm, 567 nm, and 659 nm.

The fluorescence emission spectrum of ***Z*-DPPyACN** powder with low crystallinity displayed an emission peak at 538 nm, which was seen for the molecule in chloroform solution. The gel formed by nanoparticles displayed a maximum emission at 567 nm with a shoulder at 604 nm, while the ***Z*-DPPyACN** crystal had its maximum emission at 604 nm and shoulders at 538 nm (E1) and 567 nm (E2), corresponding to the maxima emission of the powder and the gel, respectively. The red shift of the emission maximum is a function of the intermolecular interactions on the crystallinity grade or molecular aggregate, and the presence of a shoulder in the emission spectrum of the crystal at the powder and gel maxima emission highlight the importance of these interactions, *i.e.*, van der Waals forces. In addition, the crystal emission compared with the emission of ***Z*-DPPyACN** in methanol showed a similar spectrum, with a strong emission peak at 604 nm, another band of lower intensity at 538 nm, and a little shoulder at 659 nm. This result indicates that other important parameters to consider are the number of molecules in the unit cell and the size and type of crystal, *i.e.*, the environment surrounding a molecule. Because ***Z*-DPPyACN** is a charge transfer molecule, it is extremely sensitive to the environment. The lone pair of the nitrogen atom can more strongly resonate with the rings of phenyl groups than with the rest of molecule. Thus, each molecule in the crystal structure can interact such that the band corresponding to the n → π* transition shows greater spectral intensity than does a compound with -N($CH_3$) substituents (Scheme 2).

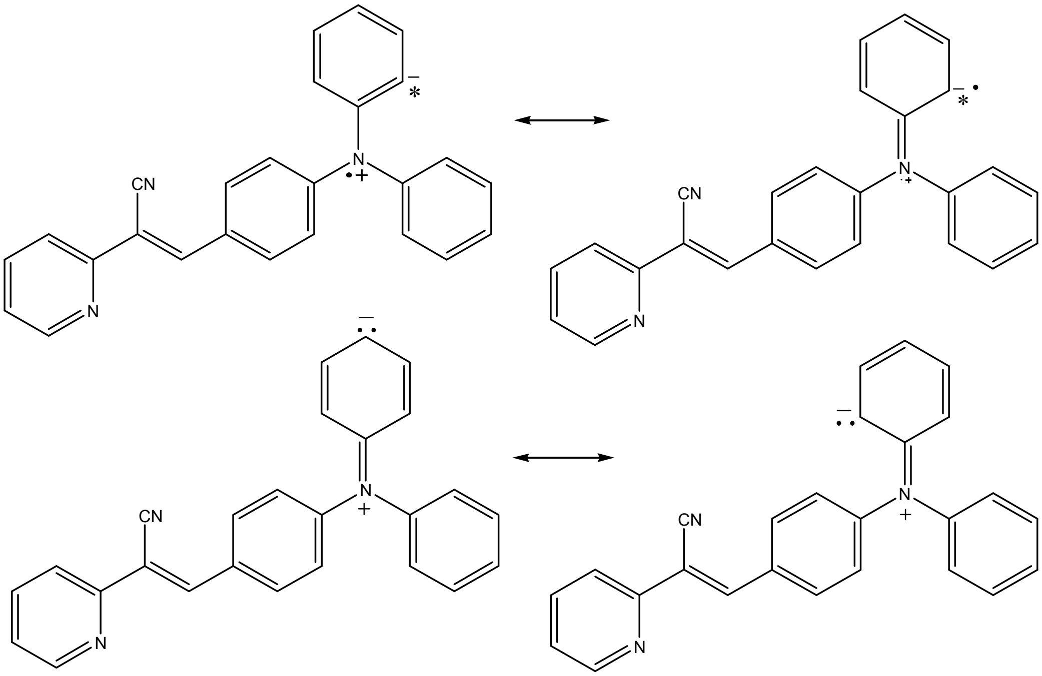

**Scheme 2.** Proposed mechanism of resonance of phenyl groups in the ***Z*-DPPyACN**.

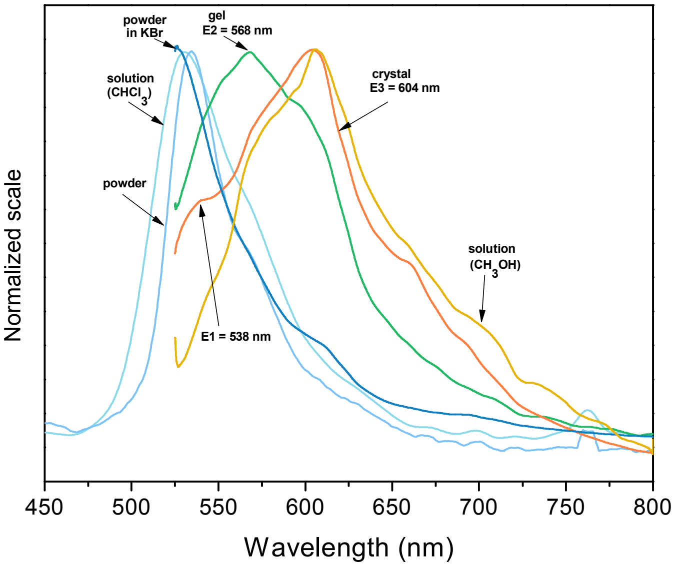

**Fig. 2** Fluorescence spectra of compound ***Z*-DPPyACN** in $CHCl_3$, solid state (KBr), aggregates as a gel (prepared using $H_2O$-THF), single crystal, and methanol solution.

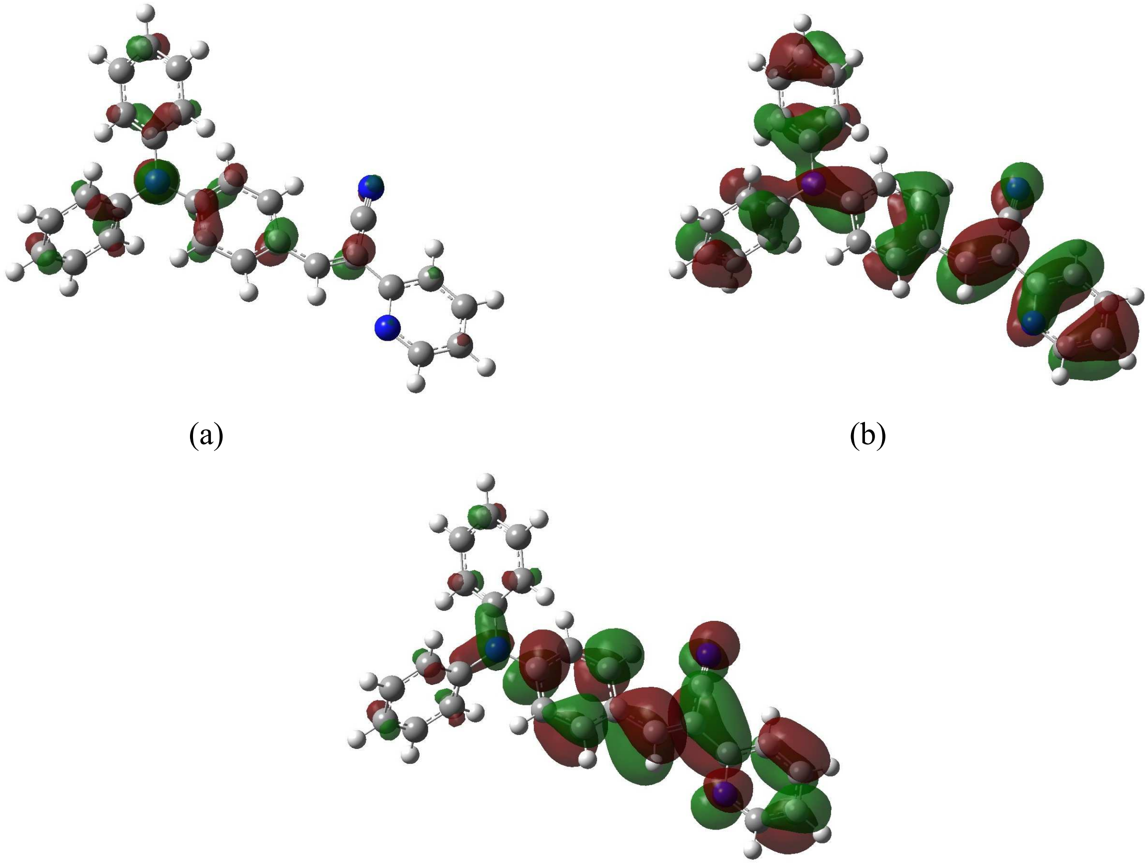
(a) (b)

(c)

**Fig. 3** Isosurfaces of the frontier molecular orbitals: (a) HOMO, (b) HOMO-1, and (c) LUMO of the ***Z*-DPPyACN** compound calculated at the B3LYP/6-31+G(d) level.

On the other hand, the emission spectrum of a single crystal of ***Z*-DPPyACN** showed three maxima at 533, 569, and 607 nm (Fig. 2). Notably, one emission band was similar to the value observed for the emission in powder at 538 nm, the second one at 569 nm corresponded to the emission from the nanoparticle (563 nm), and the last one at 607 nm corresponded to the strong emission in the crystal and in the protic polar solvent methanol (604 nm). In addition, we observed that the fluorescence emission from the single crystal was polarized along the direction to the crystal long axis. The origin of this fluorescence behavior is related to the strong polarization of the light absorption by the crystal (Fig. 4). The ratio between the absorption maximum of the z-polarized absorption and the x-polarized absorption was approximately 14, which agreed very well with the experimental emission. This effect arises from the intermolecular interactions due to the crystallization, as well as the interaction between the four molecules that form a unit cell. We performed an ORCA computational calculation using the PBE0 exchange-correlation functional of the absorption spectrum via the transition electric dipole moments between the excited state and the ground state of the four molecules in the unit cell, regardless of crystallization. This calculation showed that the transition dipole moments are mainly on the z-axis (see state $S_{12}$ in Table 2).

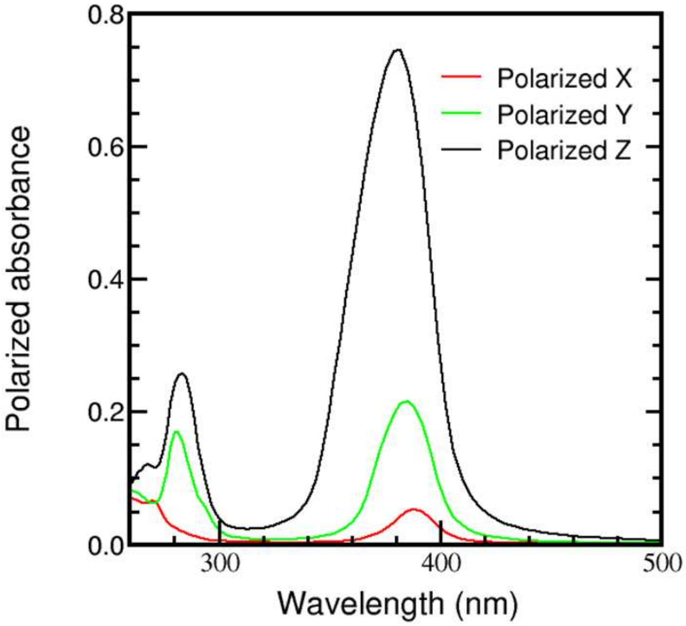

**Fig. 4** Polarized absorbance spectra from the single crystal of ***Z*-DPPyACN** using DFT *ab initio* VASP calculations at the PBE0 theory level.

The single crystal was also characterized by polarized optical microscopy (POM, Fig. 5). Careful observation of the front of the bulk material revealed the presence of an orange light of wavelength 590 nm at some parts, whereas at the side of the bulk material and at some parts of the front, the compound displayed yellow fluorescence of about 570 nm. When the crystals were crushed, their small debris presented a green light with a wavelength of about 510 nm. These results were in good agreement with those previously discussed, in that the crystals showed their emission maximum at 604 nm, while the less crystalline nanoparticles had their maximum emission at 567 nm.[82] We therefore concluded that, when the crystal breaks up, its crystallinity is reduced and this is accompanied by a change of color.[83]

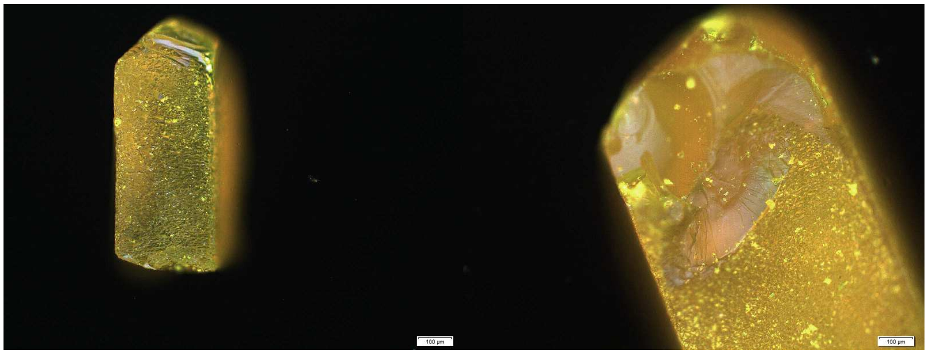

(a)

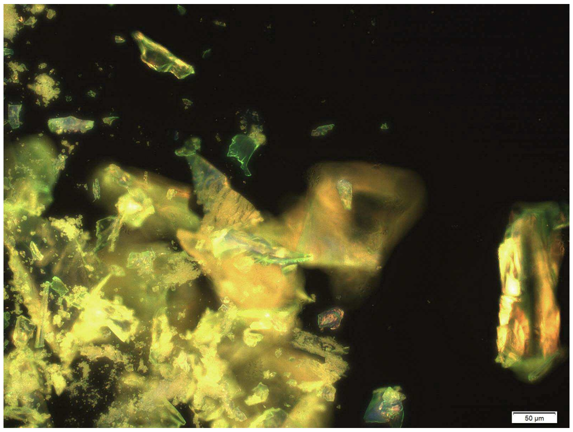

(b)

**Fig. 5** POM and polarized photoluminescence microscopy image of (a) ***Z*-DPPyACN** single crystal and (b) a crushed sample.

*Crystal and powder structure analyses*

XRSCD data for ***Z*-DPPyACN** and structure refinement are summarized in Table 3. The data were collected at 110 K. X-ray studies of single crystals were performed to demonstrate that the side-side or face-to-edge molecular stacking arrangements play important roles in the crystal packing and provide important information about the differences in optical properties. The XRSCD data showed that the compound has a ***Z***-geometry about the ethylene bridge, which links the heterocyclic and the amino aromatic rings. ***Z*-DPPyACN** belongs to the centrosymmetric space group $P2_1/n$ with $Z$= 4, where $Z$ is the number of molecules per asymmetric unit.

From these results emerged the question of whether the differences between the optical properties of the powder and the crystal were due to the presence of different phases. XRPD is a method based on the interaction of a monochromatic X-ray beam with a crystalline substance, in which the different planes of atoms or molecules in a crystal act as grating for the X-rays. The conditions required for the positive interference of the scattered X-ray beams are given by the Bragg equation, which states that, for monochromatic X-rays, the diffraction angle solely depends on the crystalline spacings. The pattern provided by XRPD (intensity *versus* scattering angle) is unique for every crystalline form of a polycrystalline sample. Therefore, XRPD is extremely useful in the identification of polymorphic forms.

Furthermore, different polymorphic or pseudopolymorphic forms exhibit peaks at different diffraction angles, i.e., they will have different crystalline spacings. The peak position, therefore, can be used to identify the polymorphic forms.

In order to find the presence of polymorph structures, we performed XRPD measurements on powder and crystalline samples of ***Z*-DPPyACN** grown from different solvents (ethanol, cyclohexane, and THF). In Fig. 6, the powder XRPD patterns show that the two forms A and B differed considerably in their peak intensities. The form A showed high intensity peaks at 2θ angles: 12.01°, 15.08°, 15.38°, 17.06°, 19.61°, 20.57°, 21.57°, 26.24°, 26.22°, and 33.94°, while form B only showed weak intensity peaks at the same positions. Additionally, the reflexes at 16.94°, 20.32°, 26.9°, and 28.7° showed a higher intensity in form B than in form A. The experimental spectra for (A) and (B) are in good agreement with the calculated spectra obtained from the experimental crystal structure (C). Data collection on the powder samples of ***Z*-DPPyACN** did not reveal the existence of additional phases.

However, the peak intensity can vary drastically depending on the orientation of the particles in the sample holder. The batches of the A and B forms of ***Z*-DPPyACN** showed differences only in the peak intensities in the XRPD diffractograms, not in the peak position (Fig. 6). Figure 6 shows that small crystals compose the powder, and they exhibit the same crystalline phase as the single crystal. Thus, both of them should show the same PL spectrum due to the number of first neighbors in the unit cell. However, their PL spectra are different and this difference could be related to the particle size. This is because a solid can be considered crystalline when the number of atoms in the volume is much larger than the number of atoms on surface, which occurs in macroscopic systems. In the case of nanocrystals, the number of atoms in the bulk is almost the same order as the number of surface atoms. The surface atoms do not obey the rule of having the same number of neighbors as those atoms in the bulk; these results affect the physical and chemical properties of nanocrystals compared with single crystals.

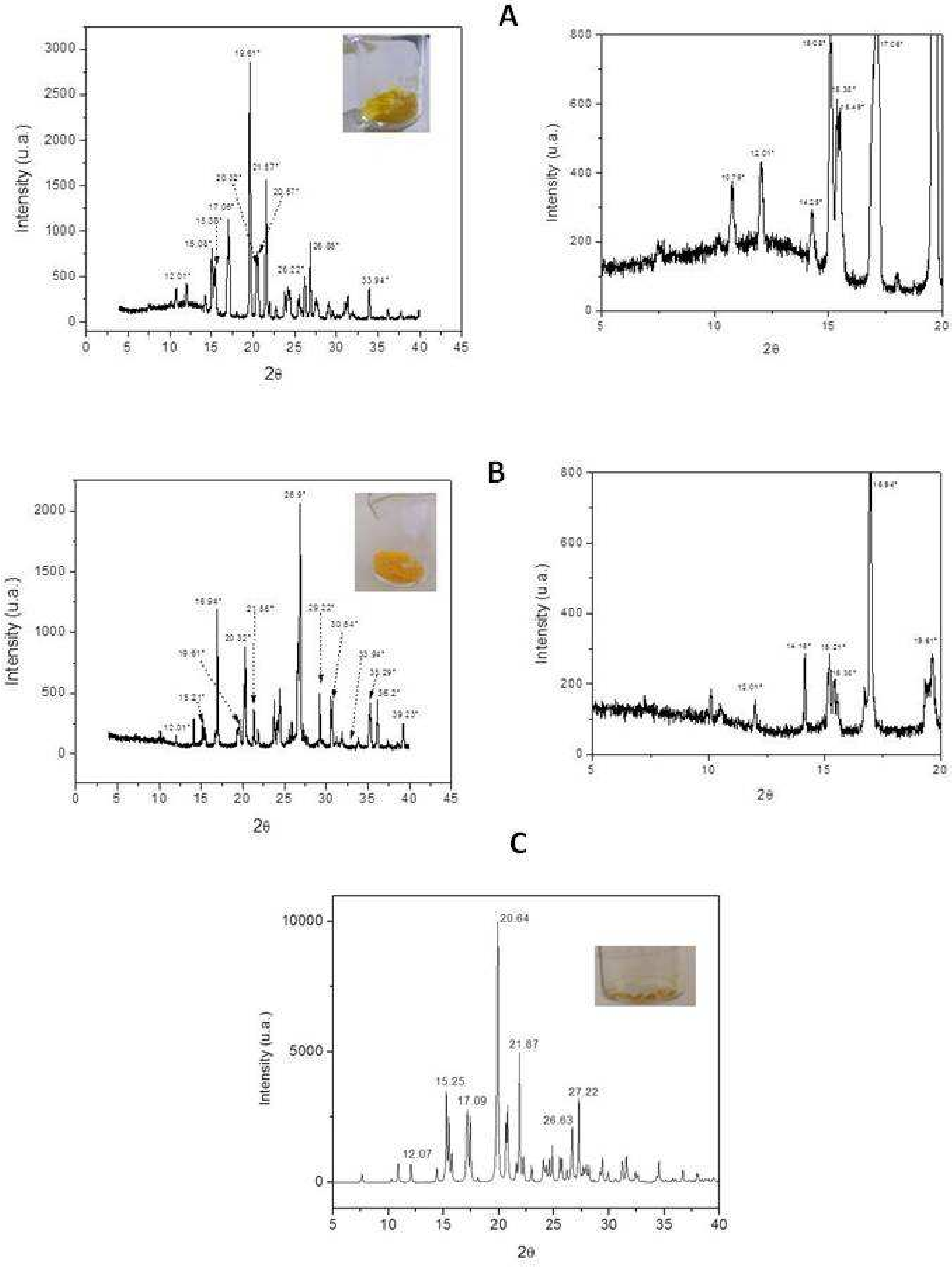

Fig. 6. XRPD diffractograms of *Z*-DPPyACN. (A) powder sample, (B) crystal sample, and (C) calculated from crystal structure data.

The molecular structure of ***Z*-DPPyACN** obtained from XRSCD data was optimized at the B3LYP/6-31+G(d) theory level (Fig. 7 and Fig. 9) to obtain the theoretical ground state molecular structure. A similar optimization was performed for the first excited state (Fig. 9). Figure 9 shows an almost planar molecule skeleton; the distances and the torsion angles between the α,β-unsaturated nitrile linkage, the pyridine ring, and the *p*-dimethylaminophenyl are shown in Table 4.

The optimized ground state structure confirmed a planar structure between the pyridine ring, the acrylonitrile linkage, and the 4-diphenylamino moiety, while the *N*,*N*-diphenyl substituents are twisted through the single bonds of the *N* atom. To corroborate the planar structure, we calculated the dihedral angle (α) between two planar individual entities, the pyridine ring and the nearest phenyl ring. The dihedral angle α between these two planes is α=17.3°, which shows that the pyridine and its nearest ring are almost coplanar. Moreover, our results are similar to those reported for *N*-methyl and *N*-phenyl substituents studied in stilbenoid systems, which displayed planar ground state geometries about the *N* atom.[11] This geometry led to a red shift of the absorption and fluorescence spectra in the *N*-phenyl substituted systems. Yang *et al.*[11] defined the sum of bond angles about the *N* atom (θ) as a criterion for the different behavior of the *N* atom when it is linked to either the *N*-alkyl or the *N*-phenyl substituent. In our case, we found that the XRSCD value (θ=359.8°) is very close to the ideal value (θ=360°). We obtained a theoretical value of θ=359.99°, which indicated a sp$^2$ character for the *N* atom in the amine.

The main calculated geometrical parameters of ***Z*-DPPyACN** in the ground and first excited states are shown in Table 4, and they were compared with the XRSCD data. The compound ***Z*-DPPyACN** showed an experimental C$sp^2$-C$sp^2$ distance for the double bond C(19)-C(20) of 1.3541(15) Å, which was very similar to the recently reported value for (*Z*)-3-(4-(dimethylamino)phenyl)-2-(pyridin-2-yl)acrylonitrile and other acrylonitrile derivatives [60,61,84,85,86]. The theoretical C(20)-C(19) double bond value (1.375 Å) of the α,β-unsaturated nitrile group in the ground state is close to the XRSCD value.

The experimental C(16)-C(19) and C(22)-C(20) ground state bond lengths of phenyl-α,β-unsaturated acrylonitrile-pyridine are 1.4524(14) Å and 1.4880(15) Å, respectively, and they correspond well to the range of a C$sp^2$–C$sp^2$ single bond, indicating a conjugated coplanar rigid backbone of ***Z*-DPPy**A**CN**. The three experimental N-C distances of the amine are similar; however, there is a slight increase in the N(1)-C(1) bond. In general, the theoretical bond lengths are larger than those determined using X-ray data, but these are in good agreement (see Table 4). From all these results, we conclude that the ***Z*-DPPyACN** molecule in the ground state presents a coplanar rigid backbone. This coplanar conjugated backbone of ***Z*-DPPyACN** could benefit from aggregates through intermolecular interactions.

From Fig. 8, we observe that a noteworthy feature of the ***Z*-DPPyACN** structure is the packing arrangement, which indicates that it is more difficult for the molecules to have π-π interactions due to the two phenyl groups attached to N(1). These are located out-of-plane with torsion angle values shown in Table 4, even though the skeleton structure composed of the pyridyl ring, double bond, and phenyl ring is almost planar, with torsion angles between atoms of C(15)-C(16)-C(19)-C(20) = 10.61(19)°, C(21)-C(20)-C(22)-C(23) = -11.81(15)°, and C(16)-C(19)-C(20)-C(21) = -2.17(18)°. The aromatic rings of the diphenyl group were closer to the pyridine and phenyl rings of the neighboring stacks, with short contacts between HC(24)···C(9) of 2.84 Å, HC(15)···HC(13) of 2.38 Å, C(3)···HC(19) of 2.87 Å, C(8)/H···πC(16) of 2.82 Å, and C(8)/H···πC(17) of 2.89 Å (Fig. 8). In addition, C-H···N (C5-H5···N3) interactions play an important role in the crystal stabilization. These interactions occur between a nitrogen atom of the pyridine ring of a ***Z*-DDPyACN** molecule and a hydrogen atom of a phenyl ring of a neighbor ***Z*-DDPyACN** molecule, with 2.84 Å distance between them. These multiple C−H···π, CH···HC, and C-H···N edge-to-face interactions are responsible for the formation of the supramolecular network between adjacent molecules.

**Table 3.** Crystallography data for (*Z*)-3-(4-(diphenylamino)phenyl)-2-(pyridin-2-yl)acrylonitrile

| Empirical formula | $C_{26}H_{19}N_3$ |
|---|---|
| Crystal system | Monoclinic |
| Color, Habit | yellow, block |
| Formula weight | 373.44 |
| Space group | $P2_1/n$ |
| T(K) | 110(2) |
| a( Å) | 12.9551(2) |
| b (Å) | 11.29300(15) |
| c (Å) | 14.6992(3) |
| β (°) | 115.648(2) |
| V ($Å^3$) | 1938.63(6) |
| Z | 4 |
| Dc(g $cm^{-3}$) | 1.279 |
| F (000) | 784 |
| μ ($mm^{-1}$) | 0.076 |
| λ (Å) | 0.71073 |
| Crystal size ($mm^3$) | 0.46× 0.38 × 0.28 |
| 2θmax(°) | 27.50 |
| N | 26191 |
| N° (I>2.0 σ(I)) | 3962 |
| R1 | 3.80 |
| wR2 | 9.72 |
| Goodness of fit | 1.066 |
| Largest diff peak and hole (e $Å^{-3}$) | 0.27 and -0.23 |

**Table 4**. Bond lengths selected in the crystal and for the ground state and first excited state of ***Z*-DPPyACN** calculated at B3LYP/6-31+G(d) theory level. Torsion angles selected in crystal structure of ***Z*-DPPyACN**

| Bond length (Å) | XRSCD data | Ground State | First Excited State | Torsion angle(°) | |
|---|---|---|---|---|---|
| N(1)-C(1) | 1.4326(13) | 1.4617 | 1.4502 | C(14)-C(13)-N(1)-C(7) | -39.35(15) |
| N(1)-C(7) | 1.4129(14) | 1.4620 | 1.4420 | C(8)-C(7)-N(1)-C(1) | -26.58(14) |
| N(1)-C(13) | 1.4041(13) | 1.4457 | 1.5041 | C(12)-C(7)-N(1)-C(13) | -23.99(16) |
| C(20)-C(19) | 1.3541(15) | 1.3753 | 1.4211 | C(18)-C(13)-N(1)-C(1) | -33.60(14) |
| C(16)-C(19) | 1.4524(14) | 1.4758 | 1.4367 | C(2)-C(1)-N(1)-C(13) | -61.26(13) |
| C(16)-C(15) | 1.4051(15) | 1.4272 | 1.4499 | C(21)-C(20)-C(22)-C(23) | -11.81(15) |
| C(16)-C(17) | 1.4035(15) | 1.4285 | 1.4515 | C(16)-C(19)-C(20)-C(22) | -2.17(18) |
| C(22)-C(20) | 1.4880(15) | 1.5154 | 1.4830 | C(15)-C(16)-C(19)-C(20) | 10.61(19) |
| C(22)-C(23) | 1.3912(15) | 1.4201 | 1.4338 | C(19)-C(20)-C(22)-N(3) | -10.65(15) |
| C(22)-N(3) | 1.3457(14) | 1.4011 | 1.4163 | | |
| C(26)-N(3) | 1.3334(15) | 1.3831 | 1.3811 | | |
| C(20)-C(21) | 1.4390(15) | 1.4601 | 1.4421 | | |
| C(21)-N(2) | 1.1512(15) | 1.2012 | 1.2048 | | |

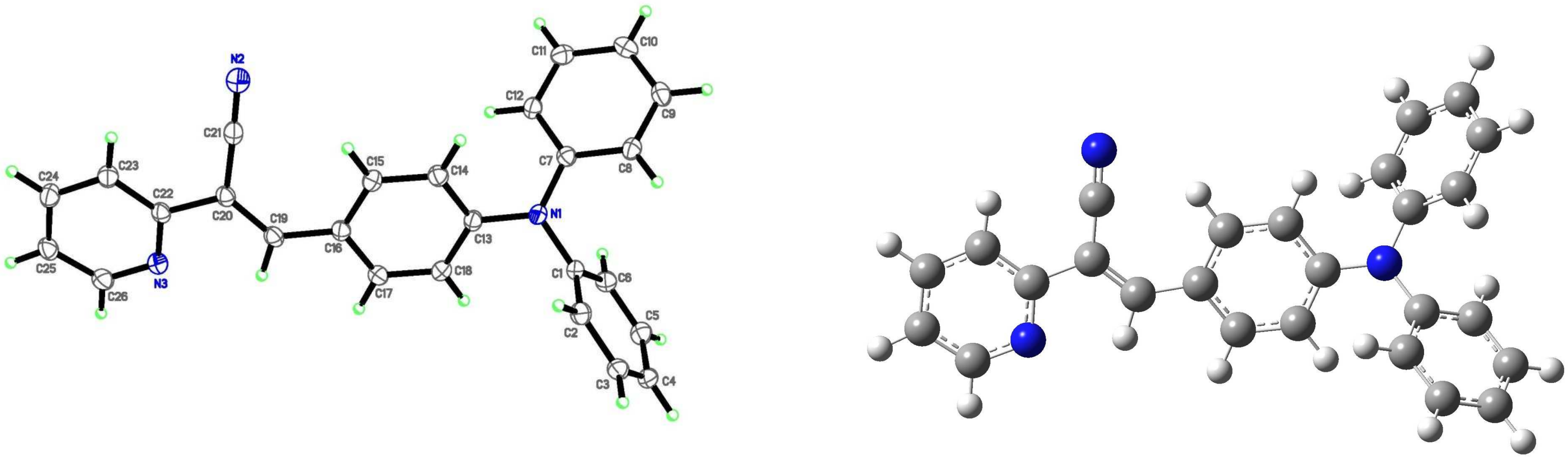

(a) (b)

**Fig. 7** Molecular structure of ***Z*-DPPyACN.** (a) ORTEP diagram with displacement ellipsoids drawn at 30% probability level and H atoms shown as small spheres of arbitrary radii. (b) The optimized structure of ***Z*-DPPyACN** calculated at the B3LYP/6-31+G(d) theory level.

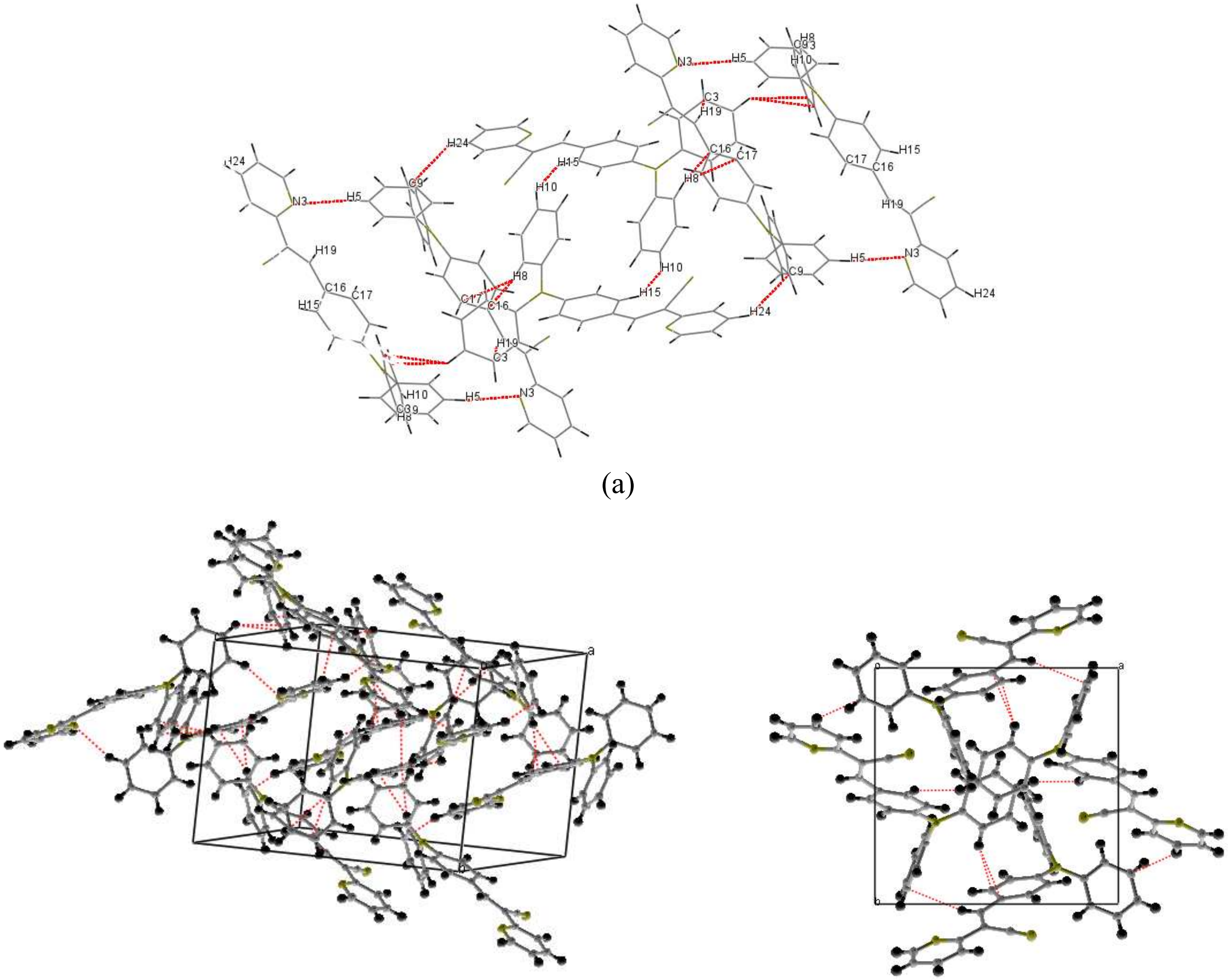

(a)

(b)

(c)

**Fig. 8** (a) C−H···π, CH···HC, and C-H···N interactions in single crystal structure of ***Z*-DPPyACN**. (b) View of the crystal packing of ***Z*-DPPyACN**. (c) Perpendicular view of unit cell showing the inversion center in the crystal structure of ***Z*-DPPyACN**.

Fig. 9 shows the optimized structures of the ground state $S_0$ and the first excited state $S_1$ of the ***Z*-DPPyACN**. The skeleton of the 3-(phenyl)-2-(pyridyl)acrylonitrile stays planar for both geometries; however, with the ground state $S_0$, the phenyl groups of *N*-diphenyl substituent are oriented 30° with respect to the planar part of the molecule. Meanwhile, in the first excited state $S_1$, the *N*-diphenyl substituent is twisted 90°, showing a perpendicular conformation between the planar skeleton and the *N*-diphenyl substituent.

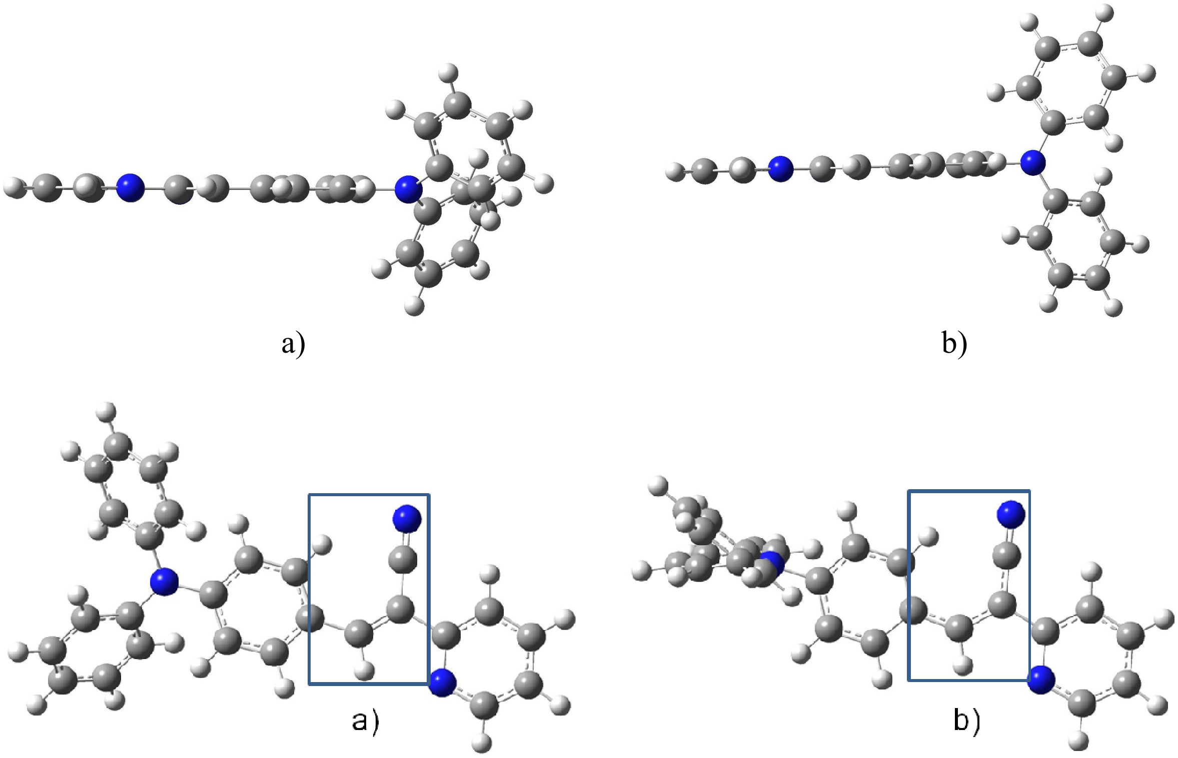

**Fig. 9** Optimized structures of (a) ground state and (b) first excited state of ***Z*-DPPyACN** calculated at B3LYP/6-31+G(d) theory level. In (a), the acrylonitrile central group has a more localized electronic distribution, while in (b), the electronic distribution has an aromatic behavior.

In addition, differential scanning calorimetry (DSC) experiments were conducted to study the thermal behavior of the two A and B forms. As shown in Fig. 10, each form exhibited a shape exothermic peak at the same temperature, which was due to the melting point of the title compound. Also, this indicated that there was no other crystalline phase, such as that detected in recent reports for different polymorphs.[87-90]

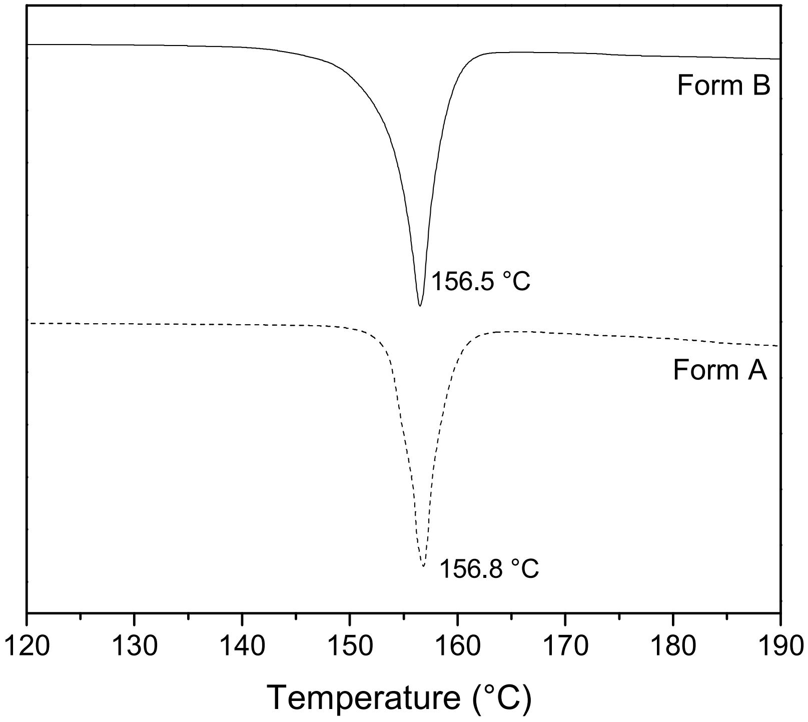

**Fig. 10.** DSC curves of A and B forms of ***Z*-DPPyACN**.

## Conclusion

The molecular basis of the luminescence behavior of bulk materials has significant importance from the point of view of their substituents, such as the diphenylamino moiety. The present study provides evidence of significant differences in the optical properties of the diphenylamino versus dimethylamine groups, specifically in their fluorescence behavior. We compared this behavior in the solid state (single crystal and powder) and in solutions using different solvents. A qualitative analysis of A and B forms of ***Z*-DPPyACN** was possible with XRPD, but did not find polymorphic phases.

The results indicated that the differences in the spectra can be caused predominantly by a transfer charge which causes the phenyl rings of the ($Ph_2N$-) to interact. The effect is observed when aggregates are formed, which also indicate a strong dependence on the structure of the compound and therefore the emission. Also, the different behavior might be attributed to the $sp^2$ and $sp^3$ character of the *N* atom of amine and therefore the better delocalization of the lone pair electron of the *N* atom. This makes that dipole in the structure different, which offsets the electrostatic repulsions that occur in solution. Even in organic nanostructures based in π-conjugated materials, the non-covalent intermolecular face-to-face π−π interactions (or π−π stacking) play an essential role in crystal engineering and the corresponding tuning of properties. In this study, it was clear that the structure did not show face-to-face π−π interactions due to cofacial configurations. Therefore, the results indicated that the role of edge-to-face interactions, termed C−H···π interactions, led to the formation of an interesting organic nanostructure with multiple C−H···π interactions. They could be applied to the engineering of nanoscale molecular assemblies and could affect their luminescent behavior. Also, theoretical calculations indicated that intermolecular interactions contribute to the understanding of the compound polarized emission, showing which emission could be due to the molecule and which could be due to the supramolecular network.

*Acknowledgment(s).* This work was supported at BUAP, UASLP, and IPICYT by SEP-PROMEP/103.5/13/2110. The authors acknowledge Dr. Maxime A. Siegler (Johns Hopkins University) for assistance with X-ray crystallography, M. Sc. Beatriz A. Rivera for technical assistance in the XRPD pattern, and LINAN at IPICYT for providing access to its facilities. The authors acknowledge Centro Nacional de Supercomputo (CNS) at IPICyT for providing access to its facilities.

## Supplementary data

The crystallographic data (excluding structure factors) reported in this paper have been deposited with the Cambridge Crystallographic Data Centre as supplementary publication no. 985348. Copies of available material can be obtained, free of charge, on application to the CCDC, 12 Union Road. Cambridge CB2 IEZ, UK, (fax: +44-(0)1223-336033 or e-mail: deposit@ccdc.cam.ac.uk).

## References

1. M. Malagoli, J. L. Brédas, *Chem. Phys. Lett.*, 2000, **327**, 13.
2. M. Malagoli, M. Manoharan, B. Kippelen, J. L. Brédas, *Chem. Phys. Lett.*, 2002, **354**, 283.
3. H. Kaji, T. Yamada, N. Tsukamoto, F. Horii, *Chem. Phys. Lett.,* 2005, **401**, 246.
4. T. Sato, K. Shizu, T. Kuga, K. Tanaka, H. Kaji, *Chem. Phys. Lett.*, 2008, **458**,152.
5. T. Yamada, H. Kaji, *J. Mol. Struct.*, 2009, **927**, 82.
6. D. M. Pai, J. F. Yanus, M. Stolka, *J. Phys. Chem.*, 1984, **88**, 4714.
7. K. Naito, A. Miura, *J. Phys. Chem.*, 1993, **97**, 6240.
8. S. Okutsu, T. Onikubo, M. Tamano, T. Enokida, *IEEE Trans Electron Devices*, **1997**, 44, 1302.
9. M. Thelakkat, C. Schmitz, C. Hohle, P. Strohriegl, H.-W. Schmidt, U. Hofmann, S. Schloter, D. Haarer, *Phys. Chem. Chem. Phys.,* 1999, **1**, 1693.
10. I. K. Yakushchenko, M. G. Kaplunov, O. N. Efimov, M. Yu Belov, S. N. Shamaev, *Phys. Chem. Chem. Phys.*, 1999, **1**, 1783.
11. J.-S. Yang, S.-Y. Chiou, K. L. Liau, *J. Am. Chem. Soc.*, 2002, **124**, 2518.
12. K. Strzelec, N. Tsukamoto, H. J. Kook, H. Sato, *Polym. Int.*, 2001, **50**, 1228.

13. X. Z. Jiang, S. Liu, M. S. Liu, P. Herguth, A. K.-Y. Jen, H. Fong, M. Sarikaya, *Adv. Funct. Mater.*, 2002, **12**, 745.
14. D. E. Loy, B. E. Koene, M. E. Thompson, *Adv. Funct. Mater.*, 2002, **12**, 245.
15. Z. Xie, B. Yang, F. Li, G. Cheng, L. Liu, G. Yang, H. Xu, L. Ye, M. Hanif, S. Liu, D. Ma, Y. Ma, *J. Am. Chem. Soc.*, 2005, **127**, 14152.
16. H. Xin, M. Guang, F. Y. Li, Z. Q. Bian, C. H. Huang, K. Ibrahim, F. Q. Liu, *Phys. Chem. Chem. Phys.*, 2002, **4**, 5895.
17. N. Satoh, J.-S. Cho, M. Higuchi, K. Yamamoto, *J. Am. Chem. Soc.*, 2003, **125**, 8104.
18. P. Strohriegl, J. V. Grazulevicius, *Adv. Mater.*, 2002, **14**, 1439.
19. J. Salbeck*, Ber. Bunsenges. Phys. Chem.*, 1996, **100**, 1667.
20. R. H. Friend, R. W. Gymer, A. B. Holmes, J. H. Burroughes, R. N. Marks, C. Taliani, D. D. C. Bradley, D. A. Dos Santos, J. L. Brédas, M. Löglund, W. R. Salaneck, *Nature*, 1999, **397**, 121.
21. M. Redecker, D. D. C. Bradley, M. Inbasekaran, W. W. Wu, E. P. Woo, *Adv. Mater.*, 1999, **11**, 241.
22. C. Ego, A. C. Grimsdale, F. Uckert, G. Yu, G. Srdanov, K. Müllen, *Adv. Mater.*, 2002, **14**, 809.
23. K. L. Tong, S. K. So, H. F. Ng, L. M. Leung, M. Y. Yeung, C. F. Lo, *Synth. Met.*, 2004, **147**, 199.
24. J. Thomas, K. R. Lin, J. T. Tao, Y.-T., C. H. Chuen, *J. Mater. Chem.*, 2002, **12**, 3516.
25. P. V. Bedworth, Y. Cai, A. Jen, S. R. Marder, *J. Org. Chem.,* 1996, **61**, 2242.
26. T. Verbiest, D. M. Burland, M. C. V. Jurich, Y. Lee, R. D. Miller, W. Volksen, *Science*, 1995, **268**, 1604.
27. S. Gilmour, A. Montgomery, R. S. R. Marder, L.-T. Cheng, A. K.-Y. Jen, Y. Cai, J. W. Perry, L. R. Dalton, *Chem. Mater.*, 1994, **6**, 1603.
28. S. R. Marder, J. W. Perry, *Science*, 1994, **263**, 1706.
29. C. M. Whitaker, E. V. Patterson, K. L. Kott, R. J McMahon, *J. Am. Chem. Soc.*, 1996, **118**, 9966.
30. C. R. Moylan, R. J. Twieg, V. Y. Lee, S. A. Swanson, K. M. Betterton, R. D. Miller, *J. Am. Chem. Soc.*, 1993, **115**, 12599.
31. K. Sakanoue, M. Motoda, M. Sugimoto, S. Sakaki, *J. Phys. Chem. A*, 1999, **103**, 5551.
32. J. Pacansky, R. J. Waltman, H. Seki, *Bull. Chem. Soc. Jpn.*, 1997, **70**, 55.
33. T. Kitamura, M. Yokoyama, *J. Appl. Phys*., 1991, **69**, 821.
34. J.-S. Yang, S.-Y. Chiou, K.-L. Liau, *J. Am. Chem. Soc*., 2002, **124**, 11.
35. C. W. Tang, S. A. Van Slyke, *Appl. Phys. Lett*., 1987, **51**, 913.
36. C. W. Tang, S. A. Van Slyke, C.H. Chen, *J. Appl. Phys.*, 1989, **65**, 3610.
37. T. Tsutsui, C. Adachi, S. Saito, *Electroluminescence in organic thin films*, in: K. Honda (Ed.), Photochemical Progress in Organized Molecular Systems, Elsevier Science Publishers B.V., Amsterdam, 1991, 71.
38. J. Kido, M. Kimura, K. Nagai, *Science*, 1995, **267**, 1332.
39. R.F. Service, *Science* 1996, **273**, 878.
40. C. Adachi, S. Tokito, T. Tsutsui, S. Sato, *Jpn. J. Appl. Phys*., 1988, **27**, 269.
41. C. Adachi, T. Tsutsui, S. Saito, *Appl. Phys. Lett.*, 1989, **55**, 1489.
42. C. Adachi, T. Tsutsui, S. Saito, *Appl. Phys. Lett.*, 1990, **56**, 799.

43. C. Adachi, T. Tsutsui, S. Saito, *Appl. Phys. Lett*., 1990, 57, 531.
44. Y. Hamada, C. Adachi, T. Tsutsui, S. Saito, *Nippon Kagaku Kaishi* 1991, **11**, 1540 (in Japanese).
45. Y. Hamada, C. Adachi, T. Tsutsui, S. Saito, *Jpn. J. Appl. Phys*., 1992, **31**, 1812.
46. W. L. Yu, J. Pei, W. Huang, A. J. Heeger, *Chem. Commun*., 2000, **8**, 681.
47. J. P. Chen, H. Tanabe, X. C. Li, T. Thoms, Y. Okamura, K. Ueno, *Synth. Met*., 2003, **132**, 173.
48. F. L. Bai, M. Zheng, G. Yu, D. B. Zhu, *Thin Solid Films* 2000, **363**, 118.
49. D. Troadec, G. Veriot, A. Moliton, *Synth. Met*., 2002, **127**, 165.
50. T. Noda, Y. Shirota, *J. Lumin*., 2000, **87–89**, 1168.
51. C. S. Ha, J. H. Shin, H. Lim, W. Cho, *J. Mater. Sci. Eng. B*, 2001, **85**, 195.
52. Z. Ning, H. Tian, *Chem. Commun*., 2009, **37**, 5483.
53. R. Sander, V. Stümpflen, J. H. Wendorff, A. Greiner, *Macromolecules*, 1996, **29**, 7705.
54. I. Janic, M. Kakas, *J. Mol. Struct*., 1984, **114**, 249.
55. Y. Sasaki, K. Kimura, M. Kubo, *J. Chem. Phys*., 1959, **31**, 477.
56. H. H. Jaffe, *J. Chem. Phys*., 1954, **22**, 1430.
57. M. Sumimoto, D. Yokogawa, M. Komeda, H. Yamamoto, *Spectrochim. Acta, Part A*, 2011, **81**, 653.
58. S. J. K. Pond, M. Rumi, M. D. Levin, T. C. Parker, D. Beljonne, M. W. Day, J.-L. Brédas, S. R. Marder, J. W. Perry, *J. Phys. Chem. A*, 2002, 106, 11470.
59. B. Wang, Y. Wang, J. Hua, Y. Jiang, J. Huang, S. Qian, H. Tian, *Chem. Eur. J.*, 2011, **17**, 2647.
60. M. J. Percino, V. M. Chapela, M. Cerón, G. Soriano-Moro, M. E. Castro, F. J. Meléndez. *J. Mol. Struc*., 2013, **1034**, 238.
61. M. J. Percino, V.M. Chapela, M. Cerón, G. Soriano-Moro, M. E. Castro, F.J. Meléndez, *Curr. Phys. Chem*., 2014, **4**, 137.
62. S.-J. Su, H. Sasabe, T. Takeda, J. Kido, *Chem. Mater*., 2008, **20**, 1691.
63. K. Tamao, M. Uchida, T. Izumizawa, K. Furukawa, S. Yamaguchiet, *J. Am. Chem. Soc*., 1996, **118**, 11974.
64. S. Dailey, M. Halim, E. Rebourt, L. E. Horsburgh, I. D. W. Samuel, A. P. Monkman, *J. Phys.: Condens. Matter,* 1998, **10**, 5171.
65. H. Sasabe, E. Gonmori, T. Chiba, Y.-J. Li, D. Tanaka, S.-J. Su, T. Takeda, Y.-J. Pu, K.-I. Nakayama, J. Kido, *Chem. Mater*., 2008, **20**, 5951.
66. C. Zhao, Z. Wang, Y. Yang, C. Feng, W. Li, Y. Li, Y. Zhang, F. Bao, Y. Xing, X. Zhang, X. Zhangd, *Cryst. Growth Des*., 2012, **12***,* 1227.
67. S. Tsuzuki, K. Honda, T. Uchimaru, M. Mikami, K. Tanabe, *J. Am. Chem. Soc*., 2002, **124**, 104.
68. W. B. Jennings, B. M. Farrell, J. F. Malone, *Acc. Chem. Res*., 2001, **34**, 885.
69. M. J. Percino, V. M. Chapela, M. Cerón, M. E. Castro, G. Soriano-Moro, E. Pérez-Gutiérrez, F. Meléndez-Bustamante, *J. Mater Sci. Res*., 2012, **1**, 181.
70. G. M. Sheldrick (1998) SHELX 97 and SHELXL 97, University of Göttingen, Germany
71. Gaussian 09, Revision A.1, M. J. Frisch, G. W. Trucks, H. B. Schlegel, G. E. Scuseria, M. A. Robb, J. R. Cheeseman, G. Scalmani, V. Barone, B. Mennucci, G. A. Petersson, H. Nakatsuji, M. Caricato, X. Li, H. P. Hratchian, A. F. Izmaylov, J. Bloino, G. Zheng, J. L. Sonnenberg, M. Hada, M. Ehara, K. Toyota, R. Fukuda, J.

Hasegawa, M. Ishida, T. Nakajima, Y. Honda, O. Kitao, H. Nakai, T. Vreven, J. A. Montgomery Jr., J. E. Peralta, F. Ogliaro, M. Bearpark, J. J. Heyd, E. Brothers, K. N. Kudin, V. N. Staroverov, R. Kobayashi, J. Normand, K. Raghavachari, A. Rendell, J. C. Burant, S. S. Iyengar, J. Tomasi, M. Cossi, N. Rega, N. J. Millam, M. Klene, J. E. Knox, J. B. Cross, V. Bakken, C. Adamo, J. Jaramillo, R. Gomperts, R. E. Stratmann, O. Yazyev, A. J. Austin, R. Cammi, C. Pomelli, J. W. Ochterski, R. L. Martin, K. Morokuma, V. G. Zakrzewski, G. A. Voth, P. Salvador, J. J. Dannenberg, S. Dapprich, A. D. Daniels, Ö. Farkas, J. B. Foresman, J. V. Ortiz, J. Cioslowski, D. J. Fox, Gaussian, Inc., Wallingford CT, 2009.

72. A. D. Becke, *J. Chem. Phys.*, 1993, **98**, 5648.
73. R. Ditchfield, W. J. Hehre J. A. Pople, *J. Chem. Phys*., 1971, **54**, 724.
74. F. Neese, *WIREs Comput. Mol. Sci.*, 2012, **2**, 73.
75. J. Perdew, K. Burke, M. Ernzerhof, *Phys. Rev. Lett.*, 1996, 77, 3865.
76. J. Heyd, G. E. Scuseria, M. Ernzerhof. *J. Chem. Phys.* 2003, **118**, 8207.
77. A. Schäfer, H. Horn, R. Ahlrichs *J. Chem. Phys.*, 1992, 97, 2571.
78. G. Kresse, J. Hafner, *Phys. Rev. B*, 1993, **47**, 558.
79. G. Kresse, J. Furthmuller, *Phys. Rev. B*, 1996, **54**, 11169.
80. P. E. Bloch, *Phys. Rev. B*, 1994, **50***,* 1758.
81. A. Marini, A. Muñoz-Losa, A. Biancardi, B. Mennucci, *J. Phys. Chem. B*, 2010, **114**, 17128.
82. X. Gu, J. Yao, G. Zhang, Y. Yan, C. Zhang, Q. Peng, Q. Liao, Y. Wu, Z. Xu, Y. Zhao, H. Fu, D. Zhang, *Adv. Funct. Mater.*, 2012, **22**, 4862.
83. T. J. Chow, R. Lin, C.-W. Ko, Y.-T. Tao, *J. Mater. Chem.*, 2002, **12**, 42.
84. V. N. Sonar, S. Parkin, P. A. Croks, *Acta Crystallogr., Sect. C: Cryst. Struct. Commun.*, 2005, **C61**, 78.
85. F. H. Allen, O. Kennard, D. G. Watson, L. Brammer, A. G. Orpen, R. Taylor, *J. Chem. Soc. Perkin Trans. 2*, 1987, S1.
86. M. J. Percino, M. Cerón, M. E. Castro, G. Soriano-Moro, V. M. Chapela, F. J. Melendez, *Chem*. *Pap.*, 2014, 68, 668.
87. J. Zhang, S. tan, J. Gao, W. Fan, Y. Gao, S. Qian, *J. Pharm. Pharmacol.*, 2013, **65**, 44.
88. V. Agafonov, B. Legendre, N. Rodier, D. Wouessidjewe, J.-M. Cense, *J. Pharm. Sci.*, 1991, **80**, 181.
89. T. A. Zeidan, J. T. Trotta, R. A. Chiarella, M. A. Oliveira, M. B. Hickey, Ö. Almarsson, J. F. Remenar, *Cryst. Growth Des.*, 2013, **13**, 2036.
90. M. J. Percino, M. Cerón, P. Ceballos, G. Soriano-Moro, M. E. Castro, V. M. Chapela, J. Bonilla-Cruz, M. Reyes-Reyes, R. López-Sandoval, M. A. Siegler. J. Mol. Struct. 2014, DOI: 10.1016/j.molstruc.2014.04.088.

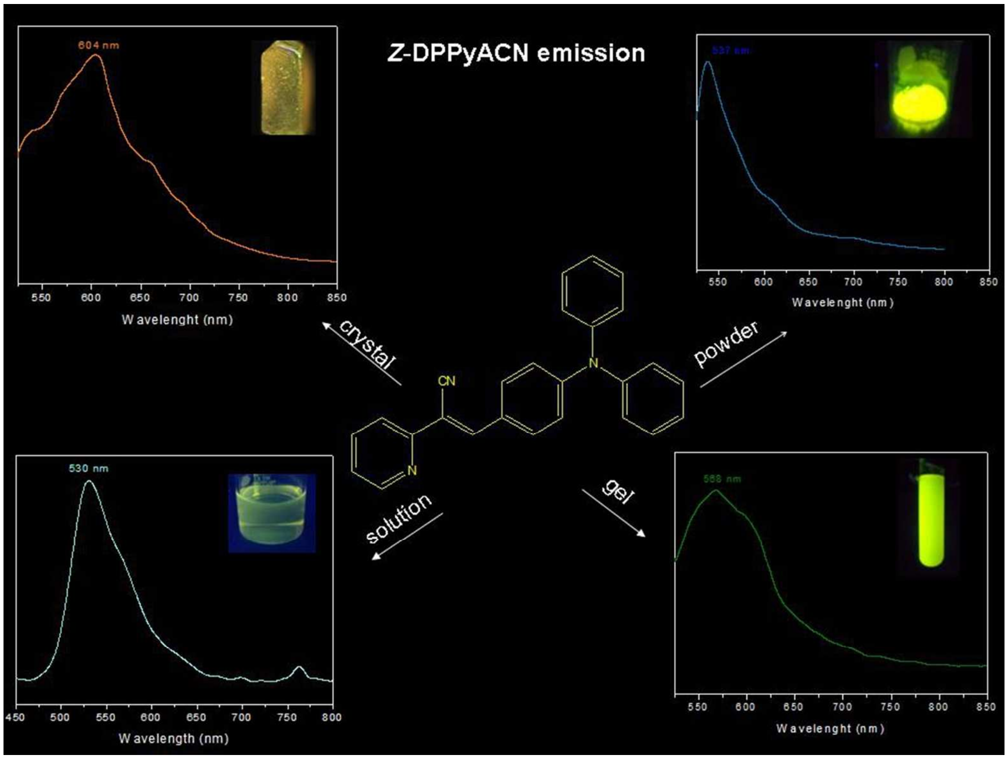

254x190mm (96 x 96 DPI)